State Observers for Output Feedback Control of an Electromagnetic Levitation System

1st Damiano Padovani
Guangdong Technion
Shantou, China
damiano.padovani@gtiit.edu.cn

2nd Andrea Cioncolini
Guangdong Technion
Shantou, China
andrea.cioncolini@gtiit.edu.cn

3rd Angelo Alessandri
Guangdong Technion and University of Genoa
Shantou, China and Genoa, Italy
angelo.alessandri@gtiit.edu.cn

***Abstract*—Electromagnetic levitation systems bring unique benefits to many fields of industry. In this context, feedback control is challenging as, in practice, only the position of the levitating object and the electromagnet current can be measured. Since we need to know all the system's state variables, including the levitating object's velocity, to ensure effective position tracking, we address the problem of constructing state observers. More specifically, we investigate a feedback linearization control scheme and design observers for output feedback by relying just on measurements of position and current. We find the observer gain by solving problems based on LMIs (linear matrix inequalities) and test our approach in simulation. The results confirm the advantage of using this control scheme with a properly selected observer gain, while considering the disturbances acting on the system.**

***Index Terms*—levitation system, position control, dynamic output feedback, observer design**

I. Introduction

Many applications of electromagnetic levitation exist, thus making this research area of particular interest in the control community. In this paper, we focus on the problem of designing state observers for dynamic output feedback to overcome the lack of velocity sensors in the feedback loop. We will place state observers in the control loop while considering the need for a convenient design, which is fundamental to set a high-precision control.

Fig. 1 depicts a sketch of an illustrative levitation system. The mass m of ferromagnetic material is subject to gravity and an electromagnetic force F_{el}, which depends on both $x_1 \geq 0$ (i.e., the distance from the electromagnet) and the intensity of the electromagnetic field, which is proportional to the square of the current flowing in the coil of the electromagnet. We have to deal with this governing equation

$$m\ddot{x}_1 = mg - F_{\text{el}} \tag{1}$$

where g denotes the gravity acceleration, and modeling F_{el} is often affected by a lot of experimental uncertainty.

Much literature on the control of levitating objects is available. In all works, the difficulty of dealing with such systems is pointed out because of the uncertainty affecting the lumped parameter model of F_{el} in (1), which is a nonlinear function of x_1 and coil current. To overcome this issue, identification is addressed as a preliminary step to control levitation systems [1], [2]. Neural networks are also adopted

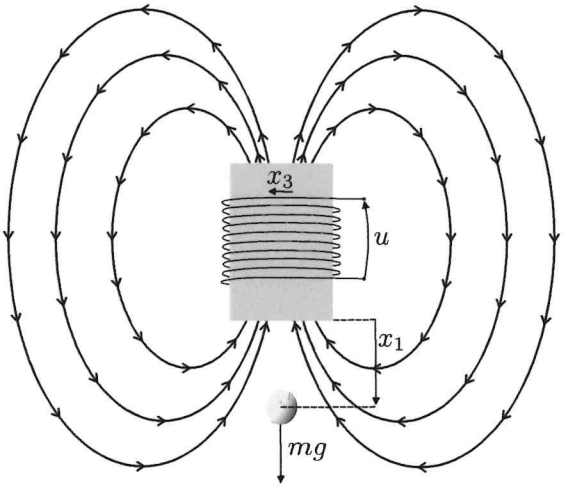

Fig. 1. Example of an explanatory levitation system.

to approximate this nonlinearity [3], [4]. While assuming knowledge of this term, the design of the position control is nontrivial in any case. In [1], the authors combine feedback linearization and PID (proportional, integral, and derivative) regulators. An internal model approach with global stability properties is presented in [5]. Model predictive control (MPC) is adopted to control a levitating mass [6]; a quadratic cost function is minimized to set the coil currents and duty cycles. In [7], an MPC-based governor selects the setpoint references of PID controllers. An adaptive approach is then presented to control a levitating object with unknown mass [8]. Suitably tuned PID regulation for position control is considered in [9], [10]. Standard LQ (linear quadratic) and PID controllers are experimentally compared in [11]. EKF (extended Kalman filter) and MPC are studied in [12] for position control while considering input saturation. Lastly, the focus is on adaptive sliding mode control in [13].

Let us now focus on the contributions of this paper. In more detail w.r.t. (1), we consider a magnetic levitation system like the one shown in Fig. 1 by using the following equations [1]:

$$\begin{aligned} \dot{x}_1 &= x_2 \\ \dot{x}_2 &= g - \varphi(x_1)\, x_3^2 \\ \dot{x}_3 &= -\tfrac{R}{L} x_3 + \tfrac{1}{L} u \end{aligned} \tag{2}$$

where the state variables x_1, x_2 represent position and velocity of the ball with mass m, x_3 is the current in the electromagnet, and u is the applied voltage; then, L and R are the winding induction and resistance, respectively. Finally, $\varphi(\cdot)$ is a decreasing function, taking different forms depending on the features of the electromagnet and the assumptions adopted to compute the field. The knowledge of $\varphi(\cdot)$ is, therefore, critical to control this system.

A crucial aspect of controlling electromagnetic levitation systems is the need to know all the state variables for feedback control, while only position and current can be measured in practice. Likewise in [14], we pursue the goal of constructing state observers specifically for a plant described by

$$\begin{cases} \dot{x}_1 = x_2 \\ \dot{x}_2 = g - \varphi(x_1)\, x_3^2 \\ \dot{x}_3 = -\frac{R}{L} x_3 + \frac{1}{L} u \\ y = (x_1\,,\, x_3) \in \mathbb{R}^2 \end{cases} \tag{3}$$

in such a way as to increase adequate closed-loop transient response and disturbance rejection. Toward this end, we will focus on state observers with linear error dynamics in a noise-free setting [15]–[17] and, later on, address the design in the presence of disturbances with an $\mathcal{L}_2$-gain approach [18]. Linear matrix inequalities (LMIs) [19] will be used to design the proposed observers. In this respect, the use of LMIs is a novel contribution compared to the state-of-the-art in control design for electromagnetic levitation systems.

The paper is organized as follows. In Section II, we present the control scheme based on feedback linearization. In Section III, we focus on the design of observers to be put in the control loop of Section II. Simulation results are reported in Section IV. Finally, conclusions are drawn in Section V together with a prospect of future work.

II. Closed-loop Control by Full State Feedback

Feedback linearization for (2) requires the knowledge of all state variables [17]. It is based on the state transformation

$$x \mapsto T(x) := \begin{pmatrix} h(x) \\ L_f h(x) \\ L_f^2 h(x) \end{pmatrix} = \begin{pmatrix} x_1 \\ x_2 \\ g - \varphi(x_1)\, x_3^2 \end{pmatrix} = \begin{pmatrix} z_1 \\ z_2 \\ z_3 \end{pmatrix}$$

for all $x \in \mathbb{R}^3$, where $z \in \mathbb{R}^3$, $x \mapsto h(x) := x_1$, and $L_f h(x)$ denotes the Lie derivative of $h(\cdot)$ with respect to the vector field given by the right-hand side of (2), i.e., $x \mapsto f(x,u) := \big(x_2\,,\, g - \varphi(x_1)\, x_3^2\,,\, -Rx_3/L + u/L\big)$. Specifically, the function $x_1 \mapsto \varphi(x_1)$ was experimentally identified in [1] resulting as follows:

$$\varphi(x_1) = \frac{1}{m(b_0 + b_1 x_1 + b_2 x_1^3 + b_3 x_1^4)}$$

with suitable parameters $b_0, b_1, b_2, b_3 \in \mathbb{R}$. Therefore, we obtain the state-space description in the z coordinates

$$\begin{pmatrix} \dot{z}_1 \\ \dot{z}_2 \\ \dot{z}_3 \end{pmatrix} = \underbrace{\begin{pmatrix} 0 & 1 & 0 \\ 0 & 0 & 1 \\ 0 & 0 & 0 \end{pmatrix}}_{A:=} \begin{pmatrix} z_1 \\ z_2 \\ z_3 \end{pmatrix} + \underbrace{\begin{pmatrix} 0 \\ 0 \\ 1 \end{pmatrix}}_{B:=} (b(x) - a(x)\, u)$$

with

$$a(x) := \frac{2x_3\, \varphi(x_1)}{L} \quad b(x) := -x_2 x_3^2 \frac{\partial \varphi(x_1)}{\partial x_1} + \frac{2R\, x_3^2\, \varphi(x_1)}{L}\,.$$

For $x \in \mathbb{R}^3$ such that $a(x) \neq 0$, we can replace u with $(b(x) - v)/a(x)$, where $v \in \mathbb{R}$ is regarded as the new control input. Thus, we get the state equation in the Brunowski form:

$$\dot{z} = A\, z + B\, v\,. \tag{4}$$

Since (A, B) is controllable, we can apply the state feedback law $v = -K\, z + r$ with $K = (K_1\,,\, K_2\,,\, K_3) \in \mathbb{R}^{1\times 3}$ chosen by means of pole placement to impose eigenvalues $A - BK$ with strictly negative real parts. Once the pole assignment is done, it is straightforward to check that the reference signal for tracking the position x_1^* is given by

$$r = R\sqrt{\frac{g}{\varphi(x_1^*)}} + K_1 x_1^* =: \kappa(x_1^*)\,.$$

The aforesaid is illustrated in Fig. 2, where for the sake of brevity $\gamma(x, v) := (b(x) - v)/a(x)$ from now on. This control scheme will be a starting point for the next section, where output feedback is addressed.

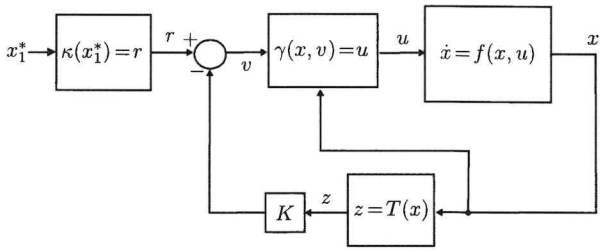

Fig. 2. State feedback control scheme.

III. Observer Design for Output Feedback

In this section, we consider the problem of constructing observers to be put in the loop of Fig. 2 in such a way as to perform output feedback by using only measurements of position and current. A possible scheme of interest is shown in Fig. 3, where the control law

$$v(t) = -K\hat{z}(t) + r(t)$$

is adopted with $\hat{z}(t) \in \mathbb{R}^3$ denoting the estimate of $z(t) \in \mathbb{R}^3$ at time $t \geq 0$ and taking

$$C = \begin{pmatrix} 1 & 0 & 0 \\ 0 & 0 & 1 \end{pmatrix}.$$

Toward this end, notice that the plant is described in the z state variables by

$$\begin{cases} \dot{z} = A\, z + B\, v \\ \bar{y} = C\, z \end{cases} \tag{5}$$

where $\bar{y} = (y_1\,,\, g - \varphi(y_1)\, y_2^2) = (x_1\,,\, g - \varphi(x_1)\, x_3^2)$. A standard linear Luenberger observer is thus given by

$$\dot{\hat{z}} = A\, \hat{z} + B\, v + L_z\, (\bar{y} - C\, \hat{z}) \tag{6}$$

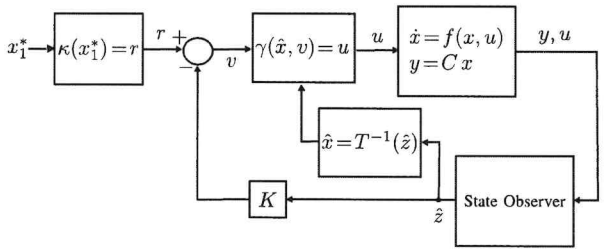

Fig. 3. Output feedback control scheme in z coordinates.

where $L_z \in \mathbb{R}^{3\times 2}$ is the observer gain to be chosen in such a way as to make $A - L_z C$ Hurwitz. This gain exists since the pair (A, C) is observable. Unfortunately, we should use the inverse mapping of $x \mapsto T(x)$, denoted by $T^{-1}(\cdot)$, which is not well defined for all $z \in \mathbb{R}^3$. This might cause some difficulties since it is not guaranteed the estimate of z to satisfy the invertibility condition of T. Therefore, we will investigate a different observer structure by referring to the x coordinates, i.e., an observer with $\hat{x} \in \mathbb{R}^3$ as state vector and the mapping $\hat{z} = T(\hat{x})$, which is well defined for all $\hat{x} \in \mathbb{R}^3$. This observer-based control scheme is shown in Fig. 4.

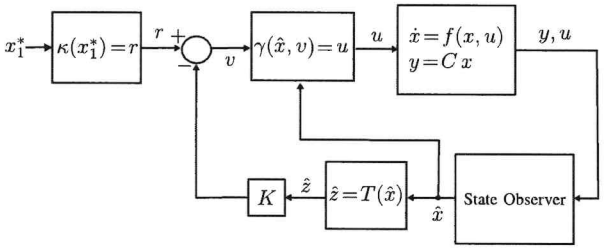

Fig. 4. Output feedback control scheme in x coordinates.

We now focus on the design of an observer for the control scheme of Fig. 4. We will not investigate the closed-loop stability of the overall control loop but the stability of the observer's estimation error, for which we will rely on an equivalent description of the plant. More specifically, we use

$$\begin{cases} \dot{x} = A\,x + \tilde{f}(x,u) \\ y = C\,x \end{cases} \tag{7}$$

with $\tilde{f}(x,u) = \big(0\,,\, g - \varphi(x_1)x_3^2\,,\, u/L\big)$,

$$A = \begin{pmatrix} 0 & 1 & 0 \\ 0 & 0 & 0 \\ 0 & 0 & -R/L \end{pmatrix}, \quad C = \begin{pmatrix} 1 & 0 & 0 \\ 0 & 0 & 1 \end{pmatrix}$$

as it is equivalent to (3). It is worth noting that the pair (A, C) of (7) is observable. Second, consider the state observer

$$\dot{\hat{x}} = A\,\hat{x} + \tilde{f}(y,u) + L\,(y - C\,\hat{x}) \tag{8}$$

where $\hat{x}(t) \in \mathbb{R}^3$ is the estimate of $x(t)$ at time $t \geq 0$, $L \in \mathbb{R}^{3\times 2}$, and $\tilde{f}(y,u)$ denotes $f((y_1, 0, y_2), u)$ with a little abuse of notation. It is straightforward to check that (8) exhibits a linear error dynamics, i.e., if we define $e(t) := x(t) - \hat{x}(t) \in \mathbb{R}^3$, we obtain $\dot{e} = (A - LC)e$, which turns out to be asymptotically stable to zero if we choose the observer gain L in such a way as to get a Hurwitz matrix $A - LC$.

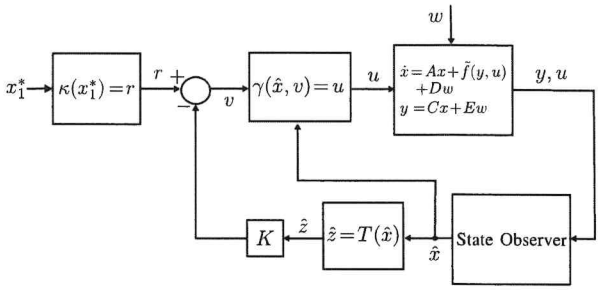

Fig. 5. Output feedback control scheme in x coordinates with a plant affected by disturbances.

Though, in principle, we can find the observer gain to guarantee the asymptotic stability of the estimation error by using some pole placement technique, it is more convenient to design the observer by considering both system and measurement noises. Thus, instead of (7), we refer to

$$\begin{cases} \dot{x} = A\,x + \tilde{f}(y,u) + D\,w \\ y = C\,x + E\,w \end{cases} \tag{9}$$

to easily account for the error dynamics, where $w \in \mathbb{R}^4$ is a vector that collects both system and measurement noises with

$$D = \begin{pmatrix} 0 & 0 & 0 & 0 \\ 1 & 0 & 0 & 0 \\ 0 & 1 & 0 & 0 \end{pmatrix}, \quad E = \begin{pmatrix} 0 & 0 & 1 & 0 \\ 0 & 0 & 0 & 1 \end{pmatrix}.$$

Specifically, w_1, w_2 in (9) account for system disturbances, whereas w_3, w_4 represent measurement noises. Thus, we obtain the error dynamics

$$\dot{e} = (A - LC)e + (D - LE)w\,, \tag{10}$$

which can be investigated in line with [18]. More specifically, we can find the observer gain L after solving the LMI problem

$$\min \delta \quad \text{w.r.t.} \quad Y, P > 0, \delta > 0 \quad \text{s.t.} \tag{11a}$$

$$\begin{pmatrix} AP - C^\top Y^\top + PA - YC + I/2 & PD - YE \\ D^\top P - E^\top Y^\top & -\delta I/2 \end{pmatrix} < 0 \tag{11b}$$

$$P > I \tag{11c}$$

aimed at minimizing the $\mathcal{L}_2$ gain involved by (10), where $Y \in \mathbb{R}^{3\times 2}$, and $P > 0$ means that $P \in \mathbb{R}^{3\times 3}$ is symmetric and positive definite. The constraint $P > I$ (i.e., $P - I > 0$) is added to ensure a well-conditioned P. Specifically, the resulting P, Y allow to get $L = P^{-1}Y$, while providing an $\mathcal{L}_2$ gain equal to $\sqrt{\delta}$. For the purpose of comparison, notice that the selection of the observer gain can be done in a noise free-setting, namely assuming $w(t) = 0$ for all $t \geq 0$, by solving the LMI problem

$$\max \lambda \quad \text{w.r.t.} \quad Y, P > \lambda I, \lambda > 0 \quad \text{s.t.} \tag{12a}$$

$$AP - C^\top Y^\top + PA - YC < 0 \tag{12b}$$

in such a way as to get a "small" gain $L = P^{-1}Y$ with a well-conditioned P. Proper conditioning of (12) is guaranteed by the constraint $P > \lambda I$.

In the next section, we will address the observer design and simulations to analyze the performance of the resulting closed-loop scheme in Fig. 5.

IV. Simulation Example

For comparison of the proposed observers, we consider a plant with $g = 9.8$ m/s^2, $R = 2\,\Omega$, $L = 1.5 \cdot 10^{-2}$ H, $m = 0.005$ kg, $b_0 = 0.0304$ s^{2}A^2/m, $b_1 = 0.7159$ s^{2}A^2/m^2, $b_2 = -0.9165$ s^{2}A^2/m^4, and $b_3 = 1.1994$ s^{2}A^2/m^5 taken from [1].

First, we focus on the state feedback control law in z coordinates for (4) by finding a suitable controller gain K. It is convenient to perform pole placement with three poles in -10 by choosing the gain

$$K = (1000 \quad 300 \quad 30)\,. \tag{13}$$

The control scheme with this gain in the state feedback will be called FSF (full state feedback).

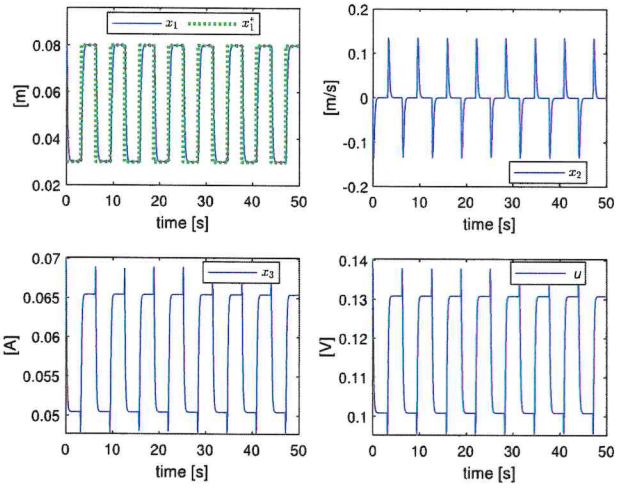

Fig. 6. Noise-free simulation run with closed-loop state feedback (FSF scheme of Fig. 2) with $x(0) = (0.08\ ,\ 0\ ,\ 0.07)$.

The solution of (12) was obtained using YALMIP [20] as follows:

$$P = \begin{pmatrix} 1.8432 & -0.2811 & 0 \\ -0.2811 & 1.8432 & 0 \\ 0 & 0 & 1.7497 \end{pmatrix} \tag{14a}$$

$$Y = \begin{pmatrix} 0.3749 & 0 \\ 1.8432 & 0 \\ 0 & -232.9206 \end{pmatrix} \tag{14b}$$

$$L = \begin{pmatrix} 0.3643 & 0 \\ 1.0556 & 0 \\ 0 & -133.1191 \end{pmatrix}. \tag{14c}$$

We refer to the observer-based control with the estimator having this gain and controller gain (13) as DOF1 (dynamic

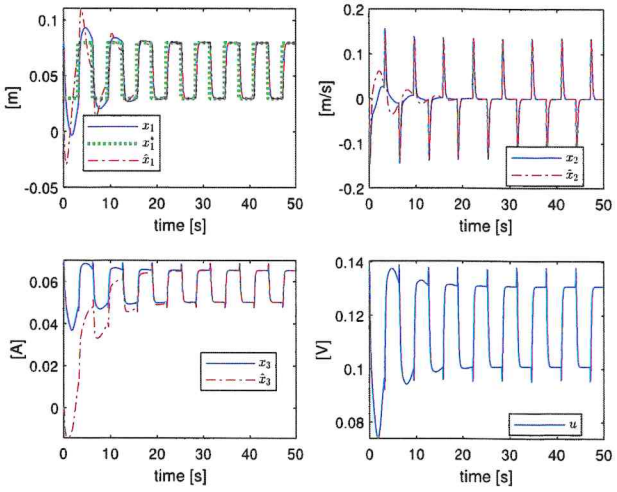

Fig. 7. Noise-free simulation run with observer-based feedback with an observer (8) having gain (14c) (DOF1 scheme of Fig. 5), $x(0) = (0.08\ ,\ 0\ ,\ 0.07)$, and $\hat{x}(0) = (0\ ,\ 0\ ,\ 0)$.

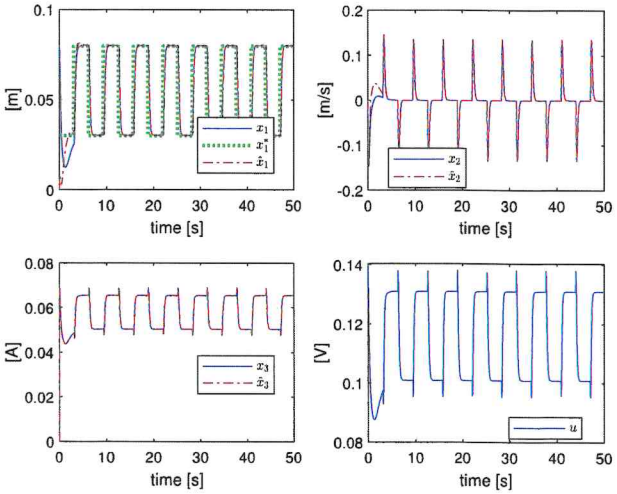

Fig. 8. Noise-free simulation run with observer-based feedback with an observer (8) having gain (15c) (DOF2 scheme of Fig. 5), $x(0) = (0.08\ ,\ 0\ ,\ 0.07)$, and $\hat{x}(0) = (0\ ,\ 0\ ,\ 0)$.

output feedback no. 1). Using again YALMIP, we solved (11) to get

$$P = \begin{pmatrix} 3.6902 & -2.8539 & 0 \\ -2.8539 & 4.0276 & 0 \\ 0 & 0 & 1.0776 \end{pmatrix} \tag{15a}$$

$$Y = \begin{pmatrix} 3.1148 & 0 \\ 2 & 0 \\ 0 & -23.1746 \end{pmatrix} \tag{15b}$$

$$L = \begin{pmatrix} 1.8675 & 0 \\ 1.3233 & 0 \\ 0 & -21.5066 \end{pmatrix}. \tag{15c}$$

We denote the observer-based control with the estimator having this gain and controller gain (13) as DOF2 (dynamic

output feedback no. 2).

In simulations that are not reported here for brevity, the DOF1 scheme showed an unstable behavior, which may be ascribed to the high gain (14c) of the observer. Thus, we relied only on the velocity estimate $\hat{x}_2$ and took y_1 and y_2 instead of $\hat{x}_1$ and $\hat{x}_3$, respectively. Thus, $(y_1\ ,\ \hat{x}_2\ ,\ y_2)$ was used in the DOF1 feedback loop with satisfying results as shown later.

Fig. 6 presents a noise-free simulation run to illustrate the behavior of the closed-loop FSF controller; the results obtained with DOF1 and DOF2 in the same simulation setting are depicted in Figs. 7 and 8. Such plots allow us to emphasize that the observer design method DOF2, based on (11), is beneficial in terms of transient response as compared to DOF1 relying on (12). The DOF2 approach tracks, in fact, the commanded position much better, ensuring smoother behavior.

In the presence of zero-mean Gaussian noises w_i, $i = 1, 2, 3, 4$ (dispersion equal to 0.0001, 0.0001, 0.0003, and 0.0003, respectively), we obtained the simulation results of Figs. 9-11. The boxplot[1] of Fig. 12 allows us to compare the input signals, where the FSF, DOF1, and DOF2 medians are equal to 0.11687, 0.11686, and 0.11689, respectively. This means that about the same actuation effort is required by the three control schemes but with very different outcomes in terms of precision, as shown in Fig. 13, where the medians of the error tracking modulus for FSF, DOF1, and DOF2 are equal to 0.00094, 0.00399, and 0.00045, respectively. Finally, Fig. 14 depicts the behavior of the tracking errors over time.

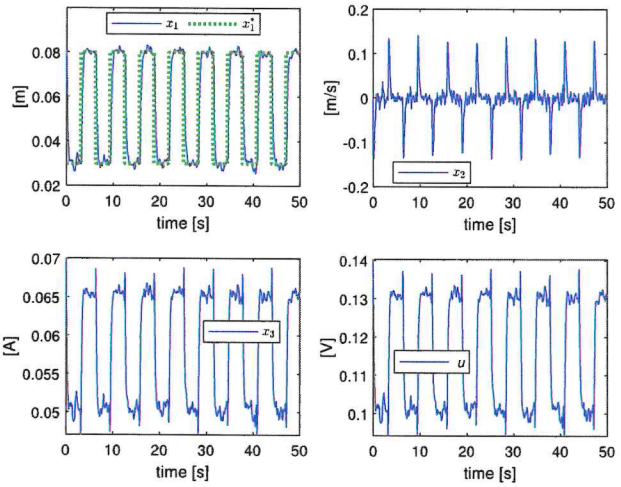

Fig. 9. Simulation run with closed-loop state feedback (FSF) with $x(0) = (0.08\ ,\ 0\ ,\ 0.07)$ and zero-mean Gaussian disturbances.

Such simulations confirm the advantage of using an observer-based feedback scheme with a properly selected observer gain, which accounts for the disturbances acting on the plant, while ensuring a satisfactory transient response.

[1]Following standard practice, the central mark indicates the median, the box sides correspond to the lower and upper quartiles, the whiskers length is 1.5 times the interquartile range, and the outliers are plotted individually using the '+' marker symbol.

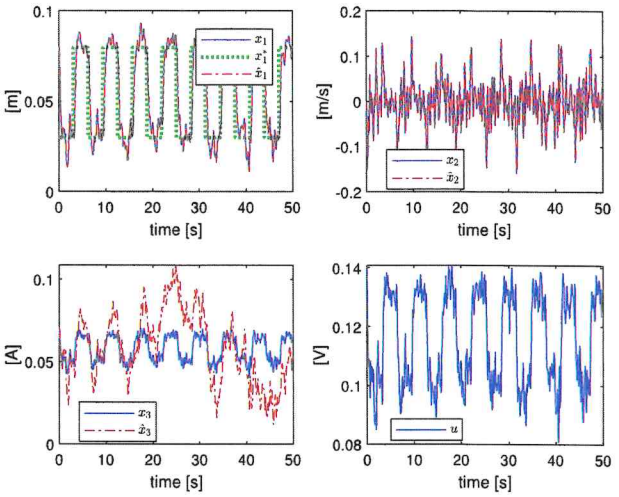

Fig. 10. Simulation run with observer-based feedback and observer (8) having gain (14c) (DOF1), $x(0) = \hat{x}(0) = (0.08\ ,\ 0\ ,\ 0.07)$, and zero-mean Gaussian disturbances.

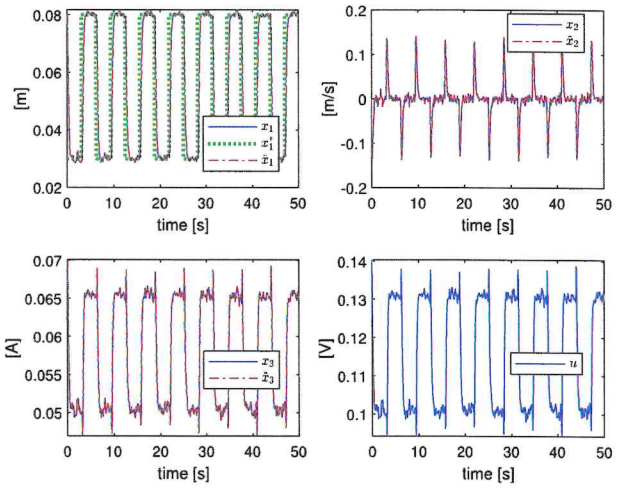

Fig. 11. Simulation run with observer-based feedback and observer (8) having gain (15c) (DOF2), $x(0) = \hat{x}(0) = (0.08\ ,\ 0\ ,\ 0.07))$, and zero-mean Gaussian disturbances.

V. Conclusions

In this paper, we tackled the design of state observers for dynamic output feedback of levitation systems without velocity measurements. We first selected the most appropriate observer structure and, second, developed a successful design method. Our design relies on using LMIs, which turns out to be effective. Future work will regard the practical verification of what we gained in simulation on an experimental setup under development. From a theoretical point of view, we will address the closed-loop stability of the observer-based control scheme. Reduced-order observers and Kalman filters will also be investigated since, in principle, we need only an estimate of the velocity of the levitating object while having measurements of position and current through sensors at our disposal.

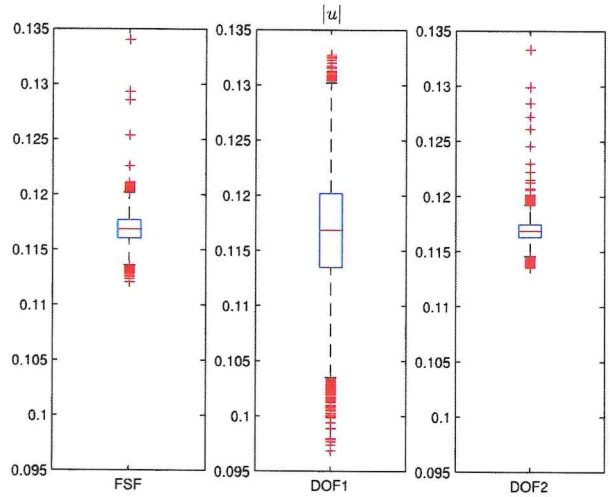

Fig. 12. Boxplots of the modulus of feedback input signals in a noisy simulation run of $1,000\,\mathrm{s}$ for FSF, DOF1, and DOF2 schemes with $x(0) = \hat{x}(0) = (0.08\ ,\ 0\ ,\ 0.07)$, and zero-mean Gaussian disturbances.

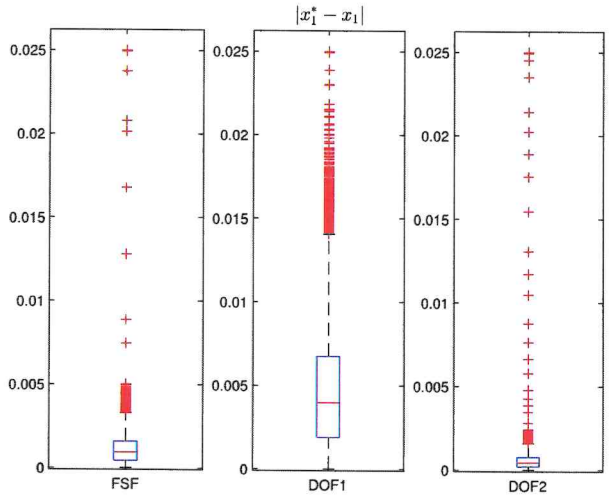

Fig. 13. Boxplots of the modulus of the tracking error in a noisy simulation run of $1,000\,\mathrm{s}$ for FSF, DOF1, and DOF2 schemes with $x(0) = \hat{x}(0) = (0.08\ ,\ 0\ ,\ 0.07)$, and zero-mean Gaussian disturbances.

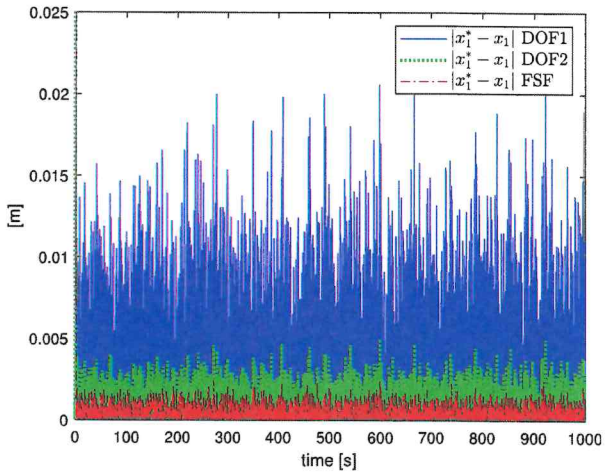

Fig. 14. Modulus of the tracking error over time in a noisy simulation run of $1,000\,\mathrm{s}$ for FSF, DOF1, and DOF2 schemes with $x(0) = \hat{x}(0) = (0.08\ ,\ 0\ ,\ 0.07)$, and zero-mean Gaussian disturbances.

References

[1] A. El Hajjaji and M. Ouladsine, "Modeling and nonlinear control of magnetic levitation systems," *IEEE Trans. on Industrial Electronics*, vol. 48, no. 4, pp. 831–838, 2001.

[2] T. Glück, W. Kemmetmüller, C. Tump, and A. Kugi, "A novel robust position estimator for self-sensing magnetic levitation systems based on least squares identification," *Control Engineering Practice*, vol. 19, no. 2, pp. 146–157, 2011.

[3] Z.-J. Yang and M. Tateishi, "Adaptive robust nonlinear control of a magnetic levitation system," *Automatica*, vol. 37, no. 7, pp. 1125–1131, 2001.

[4] Z.-J. Yang, K. Kunitoshi, S. Kanae, and K. Wada, "Adaptive robust output-feedback control of a magnetic levitation system by K-filter approach," *IEEE Trans. on Industrial Electronics*, vol. 55, no. 1, pp. 390–399, 2008.

[5] L. Gentili and L. Marconi, "Robust nonlinear disturbance suppression of a magnetic levitation system," *Automatica*, vol. 39, no. 4, pp. 735–742, 2003.

[6] T. Bächle, S. Hentzelt, and K. Graichen, "Nonlinear model predictive control of a magnetic levitation system," *Control Engineering Practice*, vol. 21, no. 9, pp. 1250–1258, 2013.

[7] M. Klaučo, M. Kalúz, and M. Kvasnica, "Real-time implementation of an explicit MPC-based reference governor for control of a magnetic levitation system," *Control Engineering Practice*, vol. 60, pp. 99–105, 2017.

[8] N. Sun, Y. Fang, and H. Chen, "Tracking control for magnetic-suspension systems with online unknown mass identification," *Control Engineering Practice*, vol. 58, pp. 242–253, 2017.

[9] C.-H. Kim, "Robust control of magnetic levitation systems considering disturbance force by LSM propulsion systems," *IEEE Trans. on Magnetics*, vol. 53, no. 11, pp. 1–5, 2017.

[10] B. Bidikli and A. Bayrak, "A self-tuning robust full-state feedback control design for the magnetic levitation system," *Control Engineering Practice*, vol. 78, pp. 175–185, 2018.

[11] M. Yaseen and H. Abd, "Modeling and control for a magnetic levitation system based on SIMLAB platform in real time," *Results in Physics*, vol. 8, pp. 153–159, 2018.

[12] K. Zhang, F. Xu, and X. Xu, "Observer-based fast nonlinear MPC for multi-DOF maglev positioning system: Theory and experiment," *Control Engineering Practice*, vol. 114, p. 104860, 2021.

[13] J. Wang, J. Rong, and J. Yang, "Adaptive fixed-time position precision control for magnetic levitation systems," *IEEE Trans. on Automation Science and Engineering*, vol. 20, no. 1, pp. 458–469, 2023.

[14] K. Afshar and A. Javadi, "Mass estimation and adaptive output feedback control of nonlinear electromagnetic levitation system," *Journal of Sound and Vibration*, vol. 495, p. 115923, 2021.

[15] A. J. Krener and A. Isidori, "Linearization by output injection and nonlinear observers," *Systems & Control Letters*, vol. 3, pp. 47–52, 1983.

[16] A. J. Krener and W. Respondek, "Nonlinear observer with linearizable error dynamics," *SIAM J. on Control and Optimization*, vol. 23, no. 2, pp. 197–216, 1985.

[17] A. Isidori, *Nonlinear Control Systems*, ser. Communications and Control Engineering. Springer London, 1995.

[18] A. Alessandri, "Lyapunov functions for state observers of dynamic systems using Hamilton–Jacobi inequalities," *Mathematics*, vol. 8, no. 2, p. 202, 2020.

[19] S. Boyd, L. El Ghaoui, E. Feron, and V. Balakrishnan, *Linear Matrix Inequalities in System and Control Theory*, ser. Studies in Applied Mathematics. Philadelphia, PA: SIAM, 1994, vol. 15.

[20] J. Löfberg, "Yalmip: A toolbox for modeling and optimization in MATLAB," in *Proceedings of the CACSD Conf.*, Taipei, Taiwan, 2004, pp. 284–289. [Online]. Available: http://users.isy.liu.se/johanl/yalmip